

Effect of Temperature and Doping on Plasmon Excitations for an Encapsulated Double-Layer Graphene Heterostructure

Godfrey Gumbs^{1,2}, Dipendra Dahal¹, and Antonios Balassis³

¹*Department of Physics and Astronomy, Hunter College of the City University of New York, 695 Park Avenue, New York, NY 10065, USA*

²*Donostia International Physics Center (DIPC), Paseo de Manuel Lardizabal 4, 20018 San Sebastián/Donostia, Spain*

³*Department of Physics & Engineering Physics, Fordham University, 441 East Fordham Road, Bronx, NY 10458, USA*

(Dated: March 8, 2022)

We perform a comprehensive analysis of the spectrum of graphene plasmons which arise when a pair of sheets are confined between conducting materials. The associated enhanced local fields may be employed in the manipulation of light on the nanoscale by adjusting the separation between the graphene layers, the energy band gap as well as the concentration of charge carriers in the conducting media surrounding the two-dimensional (2D) layers. We present a theoretical formalism, based on the calculation of the surface response function, for determining the plasmon spectrum of an encapsulated pair of 2D layers and apply it to graphene. We solve the coupled equations involving the continuity of the electric potential and discontinuity of the electric field at the interfaces separating the constituents of the hybrid structure. We have compared the plasmon modes for encapsulated gapped and gapless graphene. The associated nonlocal graphene plasmon spectrum coupled to the “sandwich” system show a linear acoustic plasmon mode as well as a low-frequency mode corresponding to in-phase oscillations of the adjacent 2D charge densities. These calculations are relevant to the study of energy transfer via plasmon excitations when graphene is confined by a pair of thick conducting materials.

PACS numbers: 73.21.-b, 71.70.Ej, 73.20.Mf, 71.45.Gm, 71.10.Ca, 81.05.ue

I. INTRODUCTION

Many researchers have been devoting a great deal of effort to exploit the unique transport and optical properties of graphene. In particular, an area of much interest to both experimentalists and theoreticians has been the study of plasmon excitations under various conditions of temperature and doping concentrations. There have been many recent works focused on the study of these plasmon modes in graphene when it is free standing¹, lying on a substrate^{2,3} or encapsulated by two conducting materials.⁴ In this paper, we investigate the way in which the plasmon mode excitations⁵ for a pair of graphene layers are affected by encapsulating conductors which are coupled non locally to the two-dimensional (2D) layers.

The unusual properties of free-standing graphene may be attributed to Bloch states in the corners of the hexagonal Brillouin zone of this 2D honeycomb crystal lattice. For example, the Dirac fermions arising from this energy band structure lead to strongly enhanced and confined local fields through dipole-dipole coupling⁶. But, recently, novel properties have been predicted when graphene electrically interacts with a nearby metallic substrate separated by a thin insulator^{7–19}. The graphene-insulator-metal plasmons have exhibited both a linear dispersion mode^{9,20} (a so-called acoustic plasmon) in the terahertz (THz) spectral regime and a plasmon mode which is 2D in nature (square root of the wave vector). Such plasmon excitations are important for improving THz sensing, signal processing on electro-optic modulation²¹ and communication technologies^{22–24}.

Reportedly, graphene encapsulated in hexagonal boron-nitride (hBN) displays an anomalous Hall effect at room temperature which may be interpreted as ballistic transport on a micrometer scale over a wide range of carrier concentration. The encapsulation makes graphene virtually protected from its surroundings but at the same time allows the use of hBN as a top gate dielectric. More generally, the properties of encapsulated graphene are currently being actively investigated due to recent advances in device fabrication techniques^{10–19,25,26}. One reason for the attention being paid to these heterostructures is the observed improvements in the electrical conductance of graphene interconnection when there is complete encapsulation by boron-nitride^{19,27–31}. Another is that when graphene interacts with a substrate such as SiC, hBN, graphite^{32–34}, an energy band gap opens up and the plasmon dispersion relation is modified.

The combination of a 2D layer interacting with a substrate presents theoreticians with a challenge to model the structure as well as to formulate the problem and eventually obtain a dispersion equation for the plasmon excitations. There already is a formulation for graphene plasmons on a substrate^{2,35,36} as well as when encapsulated by a pair

of thick conductors⁴. These works were geared to help explain the reported relevant experimental data^{37–41}. Our present investigation showed that the plasmons of an encapsulated double-layer graphene heterostructure are different in dispersive nature from the case when there are two graphene layers interacting with a single substrate.

In this paper, we present a formalism which yields the surface response function for an encapsulated pair of 2D layers. We take into account the presence of a dielectric medium separating the 2D layer from the substrate. Furthermore, the top encapsulating material could have finite thickness as shown schematically in Fig. 1. In general, this method is capable of obtaining the plasmon dispersion relation for an arbitrary number of encapsulated layers embedded within a background dielectric material which ensures that there is no electron tunneling in between the layers. In addition, our method can be extended to the case when a protective coating is placed over the top substrate. The surface response function is calculated in the vicinity of the surface and our central formula yields various already published results.^{2,42,43} This response function, thereby obtained is used to determine the plasmon modes which are exhibited as density plots. Our method includes the effect of dielectric media non locally coupled which was not investigated by Badalyan and Peeters⁴⁴ who treated the effect of the surrounding dielectric media locally. For further clarification, we compare the resulting calculated plasmon spectra for encapsulated gapless and gapped graphene in the presence and absence of the background dielectric. Besides this, we investigated the effect of temperature on the plasmon dispersion. A similar effect can be calculated for transition metal dichalcogenide monolayers, modeling them as we do for gapped graphene^{45–48}. On the other hand, the structure which we have examined here may play an important role in increasing the mobility of electrons in graphene and other 2D structure to improve the performance of nanoelectronic and spintronic devices. The plasmon mode excitation of the structure could also be used as an illumination source for imaging a sample⁴⁹ or in optoelectronic devices as a sensor.

We now outline the rest of this paper as follows. In Sec. II, we present a detailed description of our method for calculating the surface response function for a pair of 2D layers sandwiched between two conducting substrates with arbitrary separation. The calculated plasmon spectra for chosen energy band gap, carrier doping values and temperature effect are presented in Sec. III. We conclude our paper with a discussion of the highlights of our calculations in Sec. IV.

II. THEORETICAL FORMALISM

Let us consider a structure as shown in Fig. 1 where a 2D layer is placed on top of a substrate of thickness ℓ_1 with frequency-dependent dielectric function $\epsilon_1(\omega)$. Below this, there is a buffer layer between $z = \ell_1$ and $z = \ell_4$ with background dielectric constant ϵ_b and a pair of 2D layers are embedded at $z = \ell_2$ and at $z = \ell_3$. This entire structure is now placed over a thick conducting substrate of dielectric function $\epsilon_2(\omega)$ which extends from $z = \ell_4$ to infinity. For this structure we determine the surface response function which is used to calculate the plasmon frequencies.

The electrostatic potential in the vicinity of the surface for the heterostructure is written as⁵⁰

$$\phi_{<}(z) = e^{-q_{\parallel}z} - g(q_{\parallel}, \omega)e^{q_{\parallel}z}, \quad z \lesssim 0 \quad (1)$$

which introduces the surface response function $g(q_{\parallel}, \omega)$ which is the object of our calculation. To proceed further, we express the potential solutions of Poisson's equation in the various regions depicted in Fig. 1 as linear combinations of $e^{\pm q_{\parallel}z}$ by making use of the translational invariance parallel to the xy -planar interfaces.

Referring to Fig. 1, we write the potential functions in the different regions as follows:

$$\begin{aligned} \phi_{>}(z) &= a_1 e^{q_{\parallel}z} + b_1 e^{-q_{\parallel}z}, \quad 0 \leq z \leq \ell_1 \\ \phi_{1<}(z) &= t_1 e^{q_{\parallel}z} + r_1 e^{-q_{\parallel}z}, \quad \ell_1 \leq z \leq \ell_2 \\ \phi_{1>}(z) &= t_2 e^{q_{\parallel}z} + r_2 e^{-q_{\parallel}z}, \quad \ell_2 \leq z \leq \ell_3 \\ \phi_{2<}(z) &= f_1 e^{q_{\parallel}z} + k_1 e^{-q_{\parallel}z}, \quad \ell_3 \leq z \leq \ell_4 \\ \phi_{2>}(z) &= k_2 e^{-q_{\parallel}z}, \quad z \geq \ell_4 \end{aligned} \quad (2)$$

where $a_1, b_1, t_1, r_1, t_2, r_2, f_1, k_1$ and k_2 are independent of z . These are readily determined by using the continuity of the potential and the discontinuity of the electric field across the interfaces. We assume that the 2D layer at $z = 0$ has induced surface charge density σ_1 and that at $z = \ell_2$ and $z = \ell_3$ has charge density σ_2 and σ_3 , respectively. Also, using linear response theory, we have $\sigma_1 = \chi_1 \phi_{<}(0)$, $\sigma_2 = \chi_2 \phi_{1<}(\ell_2)$ and $\sigma_3 = \chi_3 \phi_{2<}(\ell_3)$, where χ_1, χ_2 and χ_3 are 2D susceptibilities. After some algebra, we can obtain the surface response function for the structure shown in Fig. 1

with the cap 2D layer. However, here we are concerned with a heterostructure without the protective layer at $z = 0$ since this simplifies our calculation and which is reasonable to neglect if ℓ_1 is large. For this, we set $\sigma_1 = 0$, $\ell_1 = d_1$, $\ell_2 = d_1 + d_2$, $\ell_3 = d_1 + d_2 + d_3$ and $\ell_4 = d_1 + d_2 + d_3 + d_4$. In this notation, we obtain $g(q_{\parallel}, \omega)$ for *two* encapsulated sheets. Setting $d_1, d_2 = d/2, d_3 = d, d_4 = d/2$, we have

$$g(q_{\parallel}, \omega) = \frac{\mathcal{N}(q_{\parallel}, \omega)}{\mathcal{D}(q_{\parallel}, \omega)}. \quad (3)$$

Here,

$$\begin{aligned} \mathcal{N}(q_{\parallel}, \omega) &= 2q_{\parallel}^2 \epsilon_0^2 \epsilon_b^2 [\sinh(q_{\parallel} d_1) N_1 + \cosh(q_{\parallel} d_1) \epsilon_1 N_2] \\ &\quad - 2 \sinh(q_{\parallel} d) N_3 N_4 \chi_2 \chi_3 + q_{\parallel} \epsilon_0 \epsilon_b [\sinh(q_{\parallel} d) N_5 \epsilon_b (\chi_2 - \chi_3) - \sinh(2q_{\parallel} d) N_6 \epsilon_b (\chi_2 + \chi_3) \\ &\quad + \cosh(2q_{\parallel} d) N_7 (\chi_2 + \chi_3) + \cosh(q_{\parallel} d) N_8 (\chi_2 + \chi_3)] \end{aligned} \quad (4)$$

with ϵ_0 denoting the permittivity of free space, for convenience we suppress the frequency-dependence of some quantities,

$$N_1 = \sinh(2q_{\parallel} d) (\epsilon_1^2 \epsilon_2 - \epsilon_b^2) + \epsilon_b (\epsilon_1^2 - \epsilon_2) \cosh(2q_{\parallel} d), \quad (5)$$

$$N_2 = (\epsilon_b^2 - \epsilon_2) \sinh(2q_{\parallel} d) + (\epsilon_2 - 1) \epsilon_b \cosh(2q_{\parallel} d), \quad (6)$$

$$N_3 = \epsilon_2 \sinh\left(\frac{q_{\parallel} d}{2}\right) + \epsilon_b \cosh\left(\frac{q_{\parallel} d}{2}\right), \quad (7)$$

$$N_4 = \epsilon_b \cosh\left(\frac{q_{\parallel} d}{2}\right) [\sinh(q_{\parallel} d_1) - \epsilon_1 \cosh(q_{\parallel} d_1)] + \epsilon_1 \sinh\left(\frac{q_{\parallel} d}{2}\right) [\cosh(q_{\parallel} d_1) - \epsilon_1 \sinh(q_{\parallel} d_1)], \quad (8)$$

$$N_5 = (\epsilon_1^2 + \epsilon_2) \sinh(q_{\parallel} d_1) - \epsilon_1 (\epsilon_2 + 1) \cosh(q_{\parallel} d_1), \quad (9)$$

$$N_6 = (\epsilon_1^2 - \epsilon_2) \sinh(q_{\parallel} d_1) + \epsilon_1 (\epsilon_2 - 1) \cosh(q_{\parallel} d_1), \quad (10)$$

$$N_7 = \sinh(q_{\parallel} d_1) (\epsilon_b^2 - \epsilon_1^2 \epsilon_2) + \epsilon_1 (\epsilon_2 - \epsilon_b^2) \cosh(q_{\parallel} d_1), \quad (11)$$

$$N_8 = \sinh(q_{\parallel} d_1) (\epsilon_1^2 \epsilon_2 + \epsilon_b^2) - \epsilon_1 (\epsilon_2 + \epsilon_b^2) \cosh(q_{\parallel} d_1), \quad (12)$$

and

$$\begin{aligned} \mathcal{D}(q_{\parallel}, \omega) &= 2q_{\parallel}^2 \epsilon_0^2 \epsilon_b^2 [\cosh(q_{\parallel} d_1) \epsilon_1 D_1 + \sinh(q_{\parallel} d_1) D_2] \\ &\quad + 2 \sinh(q_{\parallel} d) D_3 D_4 \chi_2 \chi_3 - q_{\parallel} \epsilon_0 \epsilon_b [\sinh(q_{\parallel} d) D_5 \epsilon_b (\chi_2 - \chi_3) + \sinh(2q_{\parallel} d) D_6 \epsilon_b (\chi_2 + \chi_3) \\ &\quad - \cosh(q_{\parallel} d) D_7 (\chi_2 + \chi_3) + \cosh(2q_{\parallel} d) D_8 (\chi_2 + \chi_3)] \end{aligned} \quad (13)$$

with

$$D_1 = (\epsilon_2 + \epsilon_b^2) \sinh(2q_{\parallel} d) + (\epsilon_2 + 1) \epsilon_b \cosh(2q_{\parallel} d), \quad (14)$$

$$D_2 = \sinh(2q_{\parallel}d) (\epsilon_1^2\epsilon_2 + \epsilon_b^2) + \epsilon_b (\epsilon_1^2 + \epsilon_2) \cosh(2q_{\parallel}d), \quad (15)$$

$$D_3 = \epsilon_2 \sinh\left(\frac{q_{\parallel}d}{2}\right) + \epsilon_b \cosh\left(\frac{q_{\parallel}d}{2}\right), \quad (16)$$

$$D_4 = \epsilon_b \cosh\left(\frac{q_{\parallel}d}{2}\right) [\epsilon_1 \cosh(q_{\parallel}d_1) + \sinh(q_{\parallel}d_1)] + \epsilon_1 \sinh\left(\frac{q_{\parallel}d}{2}\right) [\epsilon_1 \sinh(q_{\parallel}d_1) + \cosh(q_{\parallel}d_1)], \quad (17)$$

$$D_5 = (\epsilon_2 - \epsilon_1^2) \sinh(q_{\parallel}d_1) + \epsilon_1(\epsilon_2 - 1) \cosh(q_{\parallel}d_1), \quad (18)$$

$$D_6 = (\epsilon_1^2 + \epsilon_2) \sinh(q_{\parallel}d_1) + \epsilon_1(\epsilon_2 + 1) \cosh(q_{\parallel}d_1), \quad (19)$$

$$D_7 = \sinh(q_{\parallel}d_1) (\epsilon_1^2\epsilon_2 - \epsilon_b^2) + \epsilon_1 (\epsilon_2 - \epsilon_b^2) \cosh(q_{\parallel}d_1), \quad (20)$$

$$D_8 = \sinh(q_{\parallel}d_1) (\epsilon_1^2\epsilon_2 + \epsilon_b^2) + \epsilon_1 (\epsilon_2 + \epsilon_b^2) \cosh(q_{\parallel}d_1), \quad (21)$$

where, $\epsilon_1(\omega) = \epsilon_2(\omega) = 1 - \omega_p^2/\omega^2$ and ϵ_b is constant.

It is of interest to note that Persson⁴² calculated the surface response function for a 2D sheet lying on top of a substrate with dielectric function $\epsilon_2(\omega)$ with vacuum on the other side as

$$g_P(q_{\parallel}, \omega) = 1 - \frac{2}{1 + \epsilon_2 - \frac{\chi_3}{q_{\parallel}\epsilon_0}} \quad (22)$$

which is readily recovered from our general result in Eq. (3) by replacing $d_1 = 0$, $d = 0$ with $\chi_2 = 0$. Similarly, Hwang and Das Sarma⁴³ obtained the plasmon dispersion equation for a pair of free standing 2D layers with a chosen separation between them. When we make the substitution $\epsilon_1(\omega) = 1$, $\epsilon_2(\omega) = 1$ and $\epsilon_b = 1$ in Eq. (3), we obtain

$$g_{\text{free-standing}}(q_{\parallel}, \omega) = \frac{e^{-q_{\parallel}(3d+2d_1)} [\chi_2\chi_3 (e^{2q_{\parallel}d} - 1) - 2q_{\parallel}\epsilon_0 (\chi_2 e^{2q_{\parallel}d} + \chi_3)]}{4q_{\parallel}^2\epsilon_0^2 \left[\left(1 - \frac{\chi_2}{2q_{\parallel}\epsilon_0}\right) \left(1 - \frac{\chi_3}{2q_{\parallel}\epsilon_0}\right) - \frac{\chi_2}{2q_{\parallel}\epsilon_0} \frac{\chi_3}{2q_{\parallel}\epsilon_0} e^{-2q_{\parallel}d} \right]}. \quad (23)$$

The zeros of the denominator in Eq. (23) correspond to the plasmon poles and the resulting dispersion equation agrees with that in Ref. [43].

The dispersion equation for plasmon excitations when a 2D layer is located at some distance from the surface of a thick conducting substrate, as considered by Gumbs, et al.² can be successfully deduced from Eq. (3) by substituting $d_1 = 0$, $\chi_3 = 0$, $\epsilon_b = 1$ and $\epsilon_2 = \epsilon$. The surface response function for this case is

$$g_{\text{2D-substrate}}(q_{\parallel}, \omega) = \frac{(\epsilon - 1) (2q_{\parallel}\epsilon_0 + \chi_2) - \chi_2 (\epsilon + 1) e^{3q_{\parallel}d}}{2q_{\parallel}\epsilon_0(\epsilon + 1)e^{4q_{\parallel}d} \left[1 - \frac{\chi_2}{2q_{\parallel}\epsilon_0} \left(1 + \frac{1-\epsilon}{1+\epsilon} e^{-2q_{\parallel}\frac{3d}{2}} \right) \right]} \quad (24)$$

from which the dispersion equation is obtained by setting the factor in parenthesis in the denominator of this equation equal to zero and this agrees with the result in Ref. [2]. We emphasize that in this special case, the distance from the conducting substrate to the 2D layer is $3d/2$.

Next, we turn to the situation when there is a single 2D layer which is sandwiched between a conducting material of finite thickness on one side and by a semi-infinite conductor on the other side. The surface response function of

this structure can be deduced from Eq. (3) by setting $\chi_2 = 0$ and $d = 0$. Then the surface response function obtained is as follows:

$$g_{\text{single-layer}}(q_{\parallel}, \omega) = 1 - \frac{2 \left[(\epsilon_1 + \epsilon_2 - \frac{\chi_3}{q_{\parallel} \epsilon_0}) + (\epsilon_1 - \epsilon_2 + \frac{\chi_3}{q_{\parallel} \epsilon_0}) e^{-2q_{\parallel} d_1} \right]}{\left[(1 + \epsilon_1)(\epsilon_1 + \epsilon_2 - \frac{\chi_3}{q_{\parallel} \epsilon_0}) - (\epsilon_1 - 1)(\epsilon_1 - \epsilon_2 + \frac{\chi_3}{q_{\parallel} \epsilon_0}) e^{-2q_{\parallel} d_1} \right]}. \quad (25)$$

Equating the denominator of the second term to zero, we obtain the plasmon dispersion equation for one encapsulated layer with susceptibility χ_3 . Furthermore, if one sets χ_2 and χ_3 equal to zero in Eqs. (4) and (13), i.e., all the 2D layers in Fig. 1 are removed, we obtain an expression for the surface response function of a thick slab consisting of regions with different dielectric materials. In particular, one may then also set $\epsilon_2 = 1$, $d = 0$, $d_1 = L$ and $\epsilon_1 = \epsilon$ to obtain the surface response function for a film of thickness L given by

$$g_{\text{film}}(q_{\parallel}, \omega) = 2 \frac{g_{\infty}(q_{\parallel}, \omega)}{e^{q_{\parallel} L} - g_{\infty}^2(q_{\parallel}, \omega) e^{-q_{\parallel} L}} \sinh(q_{\parallel} L) \quad (26)$$

where $g_{\infty}(q_{\parallel}, \omega) = (\epsilon - 1)/(\epsilon + 1)$

The preceding calculations clearly confirm that our result in Eq. (3) is very useful and can be employed for a variety of structures. As we pointed out above, we may extend our calculations to include the influence of a protective top layer, as schematically demonstrated in Fig. 1. The plasmon frequency of an encapsulating substrate such as Bi_2Se_3 ⁵¹ is calculated using $\omega_p = \sqrt{n_{3D} e^2 / (\epsilon_b \epsilon_0 m^*)} = 270$ meV for $n_{3D} \approx 8.2 \times 10^{18} \text{cm}^{-3}$ and $m^* = 0.15 m_e$ representing the charge density of the conducting substrate and the effective mass of an electron given in terms of m_e , the free electron rest mass, respectively. Consequently, the background dielectric constant of a conductor can vary significantly from $\epsilon_b = 200$ –500 for barium or strontium titanate, to many orders of magnitude greater for clean, copper-based metals and the plasmon frequency may vary over a wide range up to 10^{12} Hz, which corresponds to a few meV. On the other hand, the zero temperature doping (Fermi energy) in graphene could be estimated as $E_F = \hbar v_f k_F = \hbar v_f \sqrt{\pi n_{2D}} = 0.04 \text{eV}$ ⁵² for two dimensional charge density, $n_{2D} = 10^{15} \text{m}^{-2}$ and Fermi wave vector, $k_F^{\Delta} = \sqrt{\mu^2 - \Delta^2} / \hbar v_F$ with v_F , μ and Δ as Fermi velocity, chemical potential and half band gap respectively. Thus, both quantities are of same order of magnitude, and using μ as the unit for frequency is reasonable. Now, in order to determine the plasmon modes for a pair of encapsulated 2D graphene layers numerically, the denominator, $\mathcal{D}(q_{\parallel}, \omega, T)$ in Eq. (3) is equated to zero with $\chi_2 = \chi_3 = -e^2 \Pi_{2D}^{(0)}(q_{\parallel}, \omega, T)$, where $\Pi_{2D}^{(0)}(q_{\parallel}, \omega, T)$ is the polarization function of graphene with

$$\Pi_{2D}^{(0)}(q_{\parallel}, \omega, T) = \frac{1}{2\pi^2} \int d^2 \mathbf{k} \sum_{s, s' = \pm 1} \left\{ 1 + s s' \frac{\hbar^2 v_F^2 (\mathbf{k} + \mathbf{q}) \cdot \mathbf{k} + \Delta^2}{E_k E_{|\mathbf{k} + \mathbf{q}|}} \right\} \frac{f_0(s E_k - \mu, T) - f_0(s' E_{|\mathbf{k} + \mathbf{q}|} - \mu, T)}{s E_k - s' E_{|\mathbf{k} + \mathbf{q}|} - \hbar(\omega + i0^+)}, \quad (27)$$

where, $f_0(s E_k - \mu, T) = (1 + e^{(s E_k - \mu)/k_B T})^{-1}$ is the Fermi-Dirac distribution function for subband energy, $s E_k = s \sqrt{(\hbar v_F k)^2 + \Delta^2}$ with $s = \pm 1$ and T is temperature of the system.

To investigate the effect of encapsulation on gapless and gapped graphene, we employ the polarization function of Wunsch¹ and Pyatkovskiy⁵³ respectively whereas to see the effect of temperature on the plasmon modes, we make use of the results given in Ref. [54].

III. NUMERICAL RESULTS AND DISCUSSION

In Figs. 2 and 3, we present our numerical results for nonlocal plasmon excitations of a pair of gapless and gapped graphene layers encapsulated by dielectric materials above and below them. On one side, the dielectric has finite thickness and on the other side, there is a semi-infinite material. Figure 2 portrays the plasmon modes for encapsulated double layer gapless graphene when the double layer system is in vacuum (left panel) and in background dielectric with $\epsilon_b = 2.4$ (right panel). In total, four plasmon excitation modes are obtained, two of which originating from the origin are referred as the acoustic plasmon (AP), which is linear in the wave vector at long wavelengths and has the lowest frequency, and a mode lying above it which is 2D-like that we refer to as the optical plasmon (OP). The other two plasmon modes originating from the bulk plasma frequency ω_p and the surface plasmon frequency $\omega_p/\sqrt{2}$ are labeled as the upper hybrid plasmon (UHP) and the lower hybrid plasmon (LHP), respectively. All plasmon modes survive in the longer wavelength region and get Landau damped as the mode enters the particle-hole mode region at

shorter wavelengths. Comparison of the results on the left-hand side of Fig. 2 with those on the right shows that due to embedding of the 2D layers in the dielectric background the UHP mode flattens out and becomes less dispersive. In fact, the AP mode is noticeably closer to the particle hole mode region and the range of wave vector for which this *not* Landau damped is reduced. Besides this, the embedding of graphene layers in a dielectric background leads to the separation of the AP and OP mode in the shorter wavelength region where they were merged when there was no background dielectric screening.

Figure 3 presents numerical results for encapsulated double-layer gapped graphene. The results in the left panel of these plots are for a double-layer gapped graphene system lying in vacuum and the right panel figures are for cases when the layers are embedded in a background dielectric with constant ϵ_b . As in the case of gapless graphene, when gapped graphene layers are embedded in a dielectric, we observe four plasmon modes for which an AP and OP mode originate from the origin and the other two hybrid plasmon modes, the LHP and UHP stem from the surface and bulk plasma frequencies of the substrate. A corresponding panel comparison of Fig. 2 with Fig. 3 clearly shows that due to the presence of the energy band gap, the particle-hole mode excitation region splits into two parts. The reason is due to an increase in the energy required for an electron to transfer from the valence to the conduction band. When the band gap is small of range $\Delta = 0.2\hbar\omega_p$, the splitting is not large enough for the plasmon modes to enter. However, as the band gap is increased, the splitting widens and can allow the plasmon modes originating from the bulk and surface plasma frequencies of the substrate not to undergo any Landau damping over a wide range of wave numbers. As the band gap continues to be increased, the two hybrid modes merge into one for shorter wavelengths. Beside this, we observe that when the 2D layers are embedded in a background dielectric material (right-hand side panels in the figures) the oscillator strengths of all modes become smaller and the AP mode lies closer to the particle-hole excitation region where it is Landau damped. The AP and OP modes which are degenerate in the shorter wave length region now become non-coincident when the pair of graphene layers is embedded in the dielectric background.

Our numerical calculations for the effect of temperature on the heterostructure, displayed in Fig. 4, encapsulating gapless graphene reveals that the behavior of the plasmon spectra may be affected non uniformly with respect to wave vector and frequency even at a chosen temperature. At zero temperature, the Fermi energy is equal to $0.04eV$, the corresponding Fermi temperature is $T_F \approx 450$ K and the Fermi wave vector is $k_F \approx 10^7 m^{-1}$. We may choose the plasma frequency $\omega_p \approx 10^{13} Hz$ so that we could take $T = 0.5T_F$ in our calculations. At this temperature, the electron is thermally excited and the transition between the valence band and conduction band occurs continuously causing the boundary of the single-particle excitations to smear out which is a distinct difference from that seen in Figs. 2 and 4 as an effect due to temperature. This effect due to smearing resulted in the removal of sharp boundary of the particle hole excitation region in wave vector-frequency space for which there is none at absolute zero. Due to this, the two hybrid modes originating from the vicinity of ω_p seem to be affected the most. The UHP mode dies off soon after it emerges with the bulk frequency in the long wavelength regime whereas the LHP mode survives over a wider range of wave vector and decays as $q_{||}$ is increased. The AP and OP modes survive for longer wavelength and decay in the shorter wavelength region. Also, another distinct behavior observed, when the double layer of graphene is embedded in a dielectric material is that the AP mode moves closer to the particle-hole region and becomes decayed at longer wavelengths. In addition, the AP mode and OP mode become non-degenerate in the shorter wavelength regime.

IV. CONCLUDING REMARKS

We have presented a formalism for calculating the surface response function for a layered 2D structure which is sandwiched by conducting materials. The 2D layers may be separated by dielectric materials with arbitrary thickness. Our formulation uses a transfer matrix method for explicitly calculating the electrostatic potentials and electric fields along with linear response theory for the induced charge density on the 2D layers. We could include the effect on the surface response function due to a 2D layer on the surface of the hybrid structure as illustrated in Fig. 1. However, the presence of this 2D layer was neglected in our calculations. For comparison, we have presented numerical results when the encapsulated 2D layers are not embedded in a dielectric with that when these layers have a dielectric material on either side. Our results are shown in Figs. 2 and 3 for gapless and gapped graphene, respectively. The effect due to temperature on these self-sustaining modes appears in our presented plots in Fig. 4.

These plasmons may play an important role in fundamental studies involving strong light-matter interactions on the nanoscale. Furthermore, the existence of a branch with acoustic dispersion could offer many-fold novel possibilities for the development of devices for detector, sensor and communication applications in the technologically important THz range, such as nanoscale waveguides or modulators.

We have demonstrated that we may tune the plasma frequency of a double layer graphene heterostructure by adjusting the doping concentrations. Our model calculations show that these devices have potential for high-frequency

operation and large-scale integration. We only consider high doping concentrations so that the Fermi level is far away from the Dirac \mathbf{K} point. Otherwise, localization effects on the charge carriers cannot be neglected. As a matter of fact, the broken electron-hole symmetry may be attributed to the mutual polarization of the closely spaced interacting layers and impurity scattering. The encapsulated double-layer graphene plasmons we are predicting possess strong field confinement and very low damping. This enables a new class of devices for tunable subwavelength heterostructures, strong light-matter interactions and nano-optoelectronic switches. Although all of these prospects require low plasmon damping, our model calculations show that this may be achieved if the Fermi level is not too low so that impurity scattering may be neglected.

-
- ¹ B. Wunsch, T. Stauber, F. Sols and F. Guinea New Journal of Physics, **8**, 318 (2006).
 - ² G. Gumbs, A. Iurov, and N. J. M. Horing Phys. Rev. B **91**, 235416 (2015).
 - ³ H. Liang, L. Zhang, S. Zhang, T. Cao, A. Al, S. Ruan, and C. W. Qiu, ACS Photonics, **3**(10), 1847-1853 (2016).
 - ⁴ G. Gumbs, N. J. M. Horing, A. Iurov, and D. Dahal J. Phys. D: Appl. Phys. **49** 225101 (2016).
 - ⁵ J. Song, L. Zhang, Y. Xue, Q. Y. S. Wu, F. Xia, C. Zhang, Y. L. Xiong, Y. Zhang, J. Teng, M. Premaratne, C. W. Qiu, and Q. Bao ACS Photonics, **3** (10), 1986-1992 (2016).
 - ⁶ J. D. Cox, . M. R. Singh, G. Gumbs, M. A. Anton, and F. Carreno, Phys. Rev. B **86**, 125452 (2012).
 - ⁷ B. Xiao,, K. Qin, S. Xiao, and Z. Han, Optics Commun. **355**, 602 (2015).
 - ⁸ X. Gu, I.-T. Lin, and J.-M. Liu, Applied Physics Letters **103**, 071103 (2013).
 - ⁹ T. Stauber and G. G. mez-Santos, New Journal of Physics **14**, 105018 (2012).
 - ¹⁰ A. Principi, M. Carrega, M. B. Lundeberg, A. Woessner, F. H. L. Koppens, G. Vignale, and M. Polini Phys. Rev. B **90**, 165408 (2014).
 - ¹¹ N. Kharche and S. K. Nayak, Nano Lett. **11**, 5274 (2011).
 - ¹² J. Ristein, S. Mammadov, and Th. Seyller, Phys. Rev. Lett. **108**, 246104 (2012).
 - ¹³ V. Ryzhii, A. Satou, and T. Otsuji, Jour. Appl. Phys. **101**, 024509 (2007).
 - ¹⁴ A. Woessner, M. B. Lundeberg, Y. Gao, A. Principi, P. A. Gonzlez, M. Carrega, K. Watanabe, T. Taniguchi, G. Vignale, M. Polini, J. Hone, R. Hillenbrand, and F.H. L. Koppens, Nature Materials **14**, 421 (2015).
 - ¹⁵ A. S. Mayorov, R. V. Gorbachev, S. V. Morozov, L. Britnell, R. Jalil, L. A. Ponomarenko, P. Blake, K. S. Novoselov, K. Watanabe, T. Taniguchi, and A. K. Geim, Nano Lett. **11** (6), 2396 (2011).
 - ¹⁶ M.H.D. Guimares, P.J. Zomer, J. Ingla-Ayns, J.C. Brant, N. Tombros, and B.J. van Wees Phys. Rev. Lett. **113** 086602 (2014).
 - ¹⁷ S. Yang, X. Feng, S. Ivanovici, K. Mllen, A. Chemie **49**, 8408 (2010).
 - ¹⁸ L. Britnell, R. V. Gorbachev, R. Jalil, B. D. Belle, F. Schedin, A. Mishchenko, T. Georgiou, M. I. Katsnelson, L. Eaves, S. V. Morozov, N. M. R. Peres, J. Leist, A. K. Geim, K. S. Novoselov, L. A. Ponomarenko, Science **335**, 6071 (2012).
 - ¹⁹ A. V. Kretinin, Y. Cao, J. S. Tu, G. L. Yu, R. Jalil, K. S. Novoselov, S. J. Haigh, A. Gholinia, A. Mishchenko, M. Lozada, T. Georgiou, C. R. Woods, F. Withers, P. Blake, G. Eda, A. Wirsig, C. Hucho, K. Watanabe, T. Taniguchi, A. K. Geim, and R. V. Gorbachev, Nano Lett. **14** , 3270 (2014).
 - ²⁰ A. Principi, M. Polini, and G. Vignale, Phys. Rev. B **80**, 075418 (2009).
 - ²¹ Y. Lu, J. Song, J. Yuan, L. Zhang, S. Q. Y.Wu, W. Yu, and C. Zhang, Jour. of Optical Society of America B, **33** (9), 1842-1846 (2016).
 - ²² T. Low, and P. Avouris, ACS Nano **8**, 1086 (2014).
 - ²³ P. Tassin, T. Koschny, and C. M. Soukoulis, Science **341**, 620-621 (2013).
 - ²⁴ O. Mitrofanov, I. Brener, T. S. Luk, and J. L. Reno, ACS Photonics **2**, 1763 (2015).
 - ²⁵ C. Gong, D. Hinojos, W. Wang, N. Nijem, B. Shan, R. M. Wallace, K. Cho, and Y. J. Chabal, ACS Nano **6**, 53815387 (2012).
 - ²⁶ P. V. Kamat, J. Phys. Chem. Lett., **1** (2), 520527 (2010).
 - ²⁷ N. Jain, C. A. Durcan, R. J. Gedrim, Y. Xu, and B. Yu, Nanotechnology, **24**, 355202 (2013).
 - ²⁸ H. J. Chuang, X. Tan, N. J. Ghimire, M. M. Perera, B. Chamlagain, M. M. C. Cheng, J. Yan, D. Mandrus, D. Tomanek, and Z. Zhou, Nano Lett. **14** 35943601 (2014)
 - ²⁹ C. J. Shih, Q. H. Wang, Y. Son, Z. Jin, D. Blankschtein, and M. S. Strano, ACS Nano, **8**, 5790 (2014).
 - ³⁰ T. Sun, Z. L. Wang, Z. J. Shi, G. Z. Ran, W. J. Xu, Z. Y. Wang, Y. Z. Li, L. Dai, and G. G. Qin, Applied Phys. Lett. **96**, 133301 (2010).
 - ³¹ C. R. Dean, A.F. Young, I. Meric, C. Lee, L. Wang, S. Sorgenfrei, K. Watanabe, T. Taniguchi, P. Kim, K. L. Shepard, and J. Hone Nature Nanotechnology **5**, 722 (2010).
 - ³² S. Y. Zhou , G-H Gweon, A V Fedorov , P N First , W A de Heer, D-H Lee , F. Guinea, A. H.C. Neto and A. Lanzara Nat. Mater. **6** 770 (2007).
 - ³³ N. Kharche, S. K. Nayak, Nano letters, **11**(12), 5274-5278(2011).
 - ³⁴ G. Li, A. Luican and E. Y. Andrei Physical Review Letters, **102**(17), 176804 (2009).
 - ³⁵ N. J. Horing, A. Iurov, G. Gumbs, A. Politano, and G. Chiarello (pp. 205-237), Low Dimensional and nanostructured materials and Devices, Springer International Publishing (2016).

- ³⁶ N. J. M. Horing, Phys. Rev. B **80**, 193401 (2009).
- ³⁷ A. Politano, A. R. Marino, and V. Formoso, Phys. Rev. B **84**, 033401 (2011).
- ³⁸ A. Politano, A. R. Marino, and G. Chiarello, Phys. Rev. B **86**, 085420 (2012).
- ³⁹ A. Politano, V. Formoso, and G. Chiarello, Journal of Physics: Condensed Matter, **25** (34), 345303 (2013).
- ⁴⁰ A. Politano and G. Chiarello, Applied Physics Letters, **102** (20), 201608. (2013).
- ⁴¹ A. Politano and Chiarello, Gennaro. Nanoscale, **5** (17), 8215(2013).
- ⁴² B. N. J. Persson Solid State Commun. **52**, 811-813 (1984).
- ⁴³ E. H. Hwang, S. D. Sarma Physical Review B, **80**(20), 205405(2009).
- ⁴⁴ S. M. Badalyan and F. M. Peeters, Physical Review B. **85**, 195444 (2012).
- ⁴⁵ Y. Gong, Z. Liu, A. R. Lupini, G. Shi, J. Lin, S. Najmaei, Z. Lin, A. L. Elias, A. Berkdemir, G. You, and H. Terrones, Nano letters **14**, 442 (2013).
- ⁴⁶ M. Chhowalla, H. S. Shin, G. Eda, L. J. Li, K. P. Loh, and H. Zhang, Nature Chemistry, **5**, 263 (2013).
- ⁴⁷ M. M. Ugeda, A. J. Bradley, S. F. Shi, H. Felipe, Y. Zhang, D. Y. Qiu, and F. Wang, Nature materials **13**, 1091 (2014).
- ⁴⁸ Y. H. Ho, W. P. Su, and M. F. Lin, RSC Adv. **5**, 20858 (2015).
- ⁴⁹ X. Zeng, M. Al-Amri and M. S. Zubairy, Physical Review B, **90**(23), 235418 (2014).
- ⁵⁰ G. Gumbs and N. J. M. Horing, Phys. Rev. B **43**, 2119 (1991).
- ⁵¹ A. Politano , V. M. Silkin, I. A. Nechaev, M. S. Vitiello, L. Viti, Z. S. Aliev, M. B. Babanly, G. Chiarello, P. M. Echenique, and E. V. Chulkov. Phys. Rev. Lett. **115**, 216802 (2015).
- ⁵² S. D. Sarma and Q. Li, Phys. Rev. B, **87**, 235418 (2013)
- ⁵³ P. K. Pyatkovskiy Journal of Physics: Condensed Matter, **21**, 025506 (2008).
- ⁵⁴ M. Ramezanali, M. M. Vazifeh, R. Asgari, M. Polini, A. H. MacDonald Journal of Physics A: Mathematical and Theoretical, **42**(21), 214015 (2009).

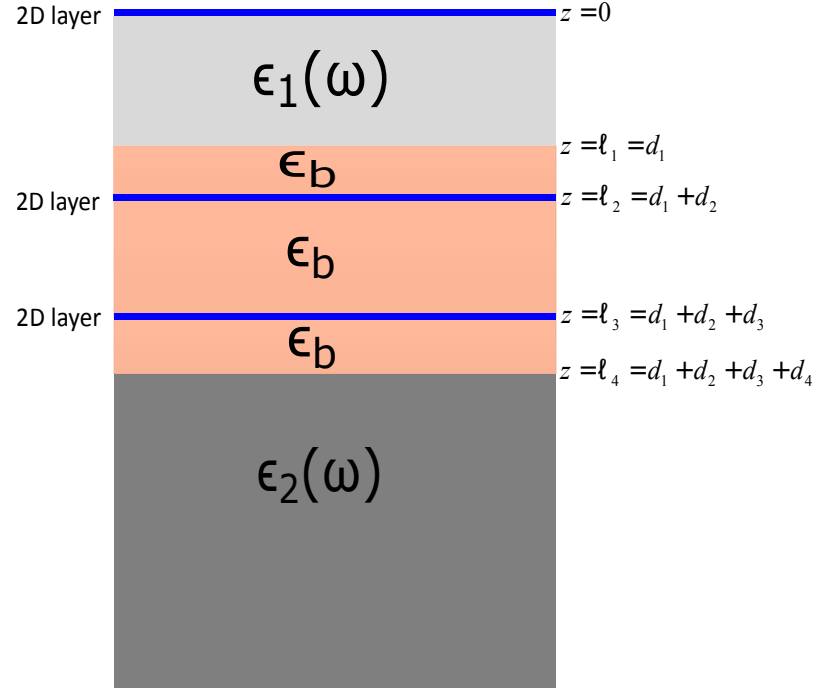


FIG. 1: (Color online) Schematic illustration of a pair of 2d layer at $z = \ell_2$ and at $z = \ell_3$ embedded in the background dielectric material of dielectric constant ϵ_b and encapsulated by conducting substrate of dielectric function $\epsilon_1(\omega)$ and $\epsilon_2(\omega)$. A protective coat of 2d layer lies on top of this heterostructure at $z = 0$.

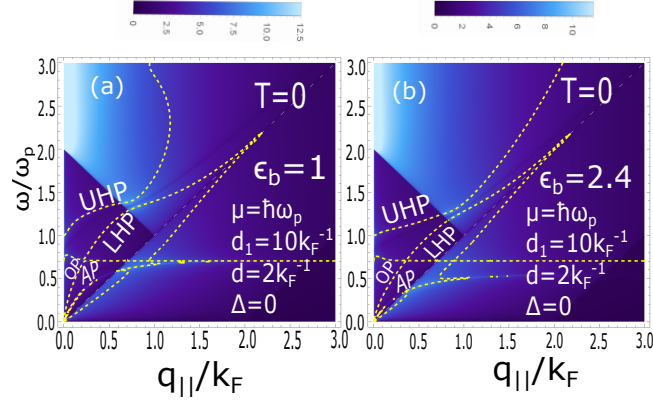


FIG. 2: (Color online) Panel(a) and (b) present density plots at zero temperature of the plasmon dispersion relation for a double layer *gapless*, doped graphene structure inserted in (a) vacuum with background dielectric constant $\epsilon_b = 1$ and (b) dielectric with background dielectric constant $\epsilon_b = 2.4$ and sandwiched between two conducting plasmas, one with finite thickness and another which is semi-infinite. The dashed lines in the dark regions show the plasma resonance for chosen values of the chemical potential μ , dielectric thickness d_1 and inter-layer separation d . Also, k_F is the Fermi wave vector for graphene. An acoustic plasmon (AP), optical plasmon (OP) and two high-frequency modes labeled as a lower hybrid plasmon (LHP) and upper hybrid plasmon (UHP) also appear in the excitation spectrum.

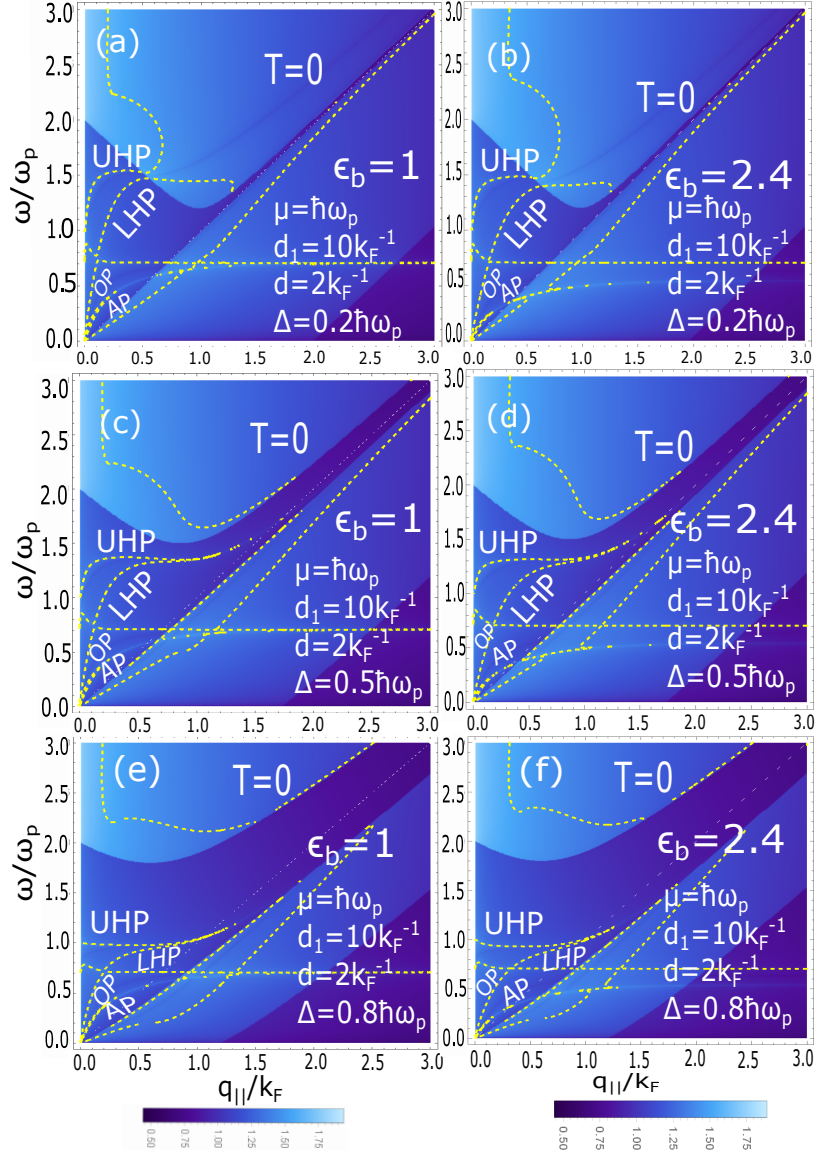


FIG. 3: (Color online) The same as in Fig. 2, except that the half-band energy gap is *finite*. In (a) and (b), $\Delta=0.2\hbar\omega_p$, for (c) and (d) $\Delta=0.5\hbar\omega_p$ and for (e) and (f) $\Delta=0.8\hbar\omega_p$. The 2D layers lie in vacuum for the left panels and in background dielectric constant $\epsilon_b = 2.4$ for right panels.

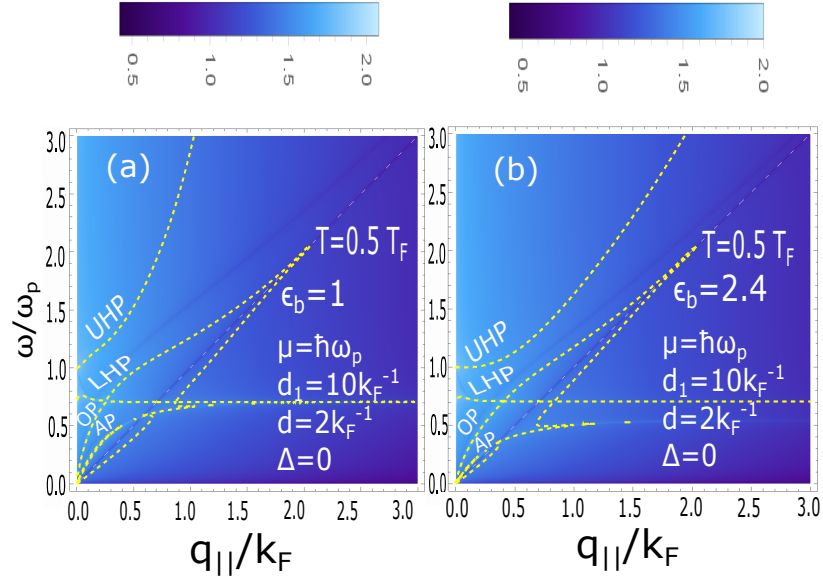


FIG. 4: (Color online) The same as in Fig. 2. except that $T = 0.5T_F$ for a pair of graphene sheets lying in vacuum(left panel) and in background dielectric constant $\epsilon_b = 2.4$ (right panel).